

## Contact Line Instabilities of Thin Liquid Films

Javier A. Diez

*Instituto de Física Arroyo Seco, Universidad Nacional del Centro de la Provincia de Buenos Aires, Pinto 399, 7000, Tandil, Argentina*

L. Kondic

*Department of Mathematical Sciences and Center for Applied Mathematics and Statistics, New Jersey Institute of Technology, Newark, New Jersey 07102*  
 (Received 5 July 2000)

We present results of fully nonlinear time-dependent simulations of a thin liquid film flowing down an inclined plane. Within the lubrication approximation, and assuming complete wetting, we find that varying the inclination angle considerably modifies the shape of the emerging patterns (fingers versus sawtooth). Our results strongly suggest that the shape of the patterns is not necessarily related to either partial or complete coverage of the substrate, a technologically important feature of the flow. We find quantitative agreement with reported experiments and suggest new ones.

DOI: 10.1103/PhysRevLett.86.632

PACS numbers: 47.15.Gf, 47.20.Ky, 47.20.Ma, 68.15.+e

The flow of thin films is relevant in a number of different fields, such as engineering (microchip production), biology (lining of mammalian lungs), and chemistry (flow of surface active materials). These flows can be driven by gravitational forces (flow down an inclined plane [1–5]), centrifugal force (spin coating [6]), thermal gradients, or Marangoni forces [7]. In all these different settings, the dynamics of the fronts of these films is not very well understood. In many situations, the fronts become unstable, leading to the formation of fingerlike rivulets, triangular sawtooth patterns, or, in the case of surfactant flow, dendritic tip-splitting petals. Very often, these instabilities are undesirable in technological applications, since they might lead to the formation of dry regions. From a more fundamental point of view, one wishes to understand the dynamics of these strongly nonlinear systems, and reach general conclusions concerning instabilities.

In this Letter, we concentrate on perhaps the simplest of these problems, the flow of a thin film of a completely wetting fluid down an inclined plane. Better understanding of this problem will provide a basic building block in assessing the issues relevant to more involved experimental setups and technological configurations. Our approach to this problem is computational: we solve numerically the partial differential equation (PDE) which governs the fluid motion. Improvement in computational methods permits us to, for the first time, accurately predict the dynamics of large systems, in computational domains which compare well with experimental ones. Our results allow for new insight into the nature of the instability, in particular, related to partial versus total coverage of the substrate, and to the shape of the emerging patterns.

The basic experimental picture is that the contact line becomes unstable with respect to transverse perturbations [1–5]. It has been conjectured that this instability is re-

lated to the formation of a capillary ridge in the fluid profile, just behind the advancing contact line. There are two important factors which influence the instability and the pattern formation process. (1) Inclination angle: Flow down a steeper incline is more susceptible to instabilities, and (2) contact angle: the fluids characterized by different wetting properties could lead to formation of different patterns and to a different degree of surface coverage [1]. Recent, well-controlled experiments [4,5] emphasize that it is still not clear how exactly these two factors influence the dynamics.

The linear stability analysis (LSA) [8–10] recovered the fact that there is a band of unstable modes, with short wavelengths stabilized by surface tension. While a basic agreement with the experimental results has been reached (e.g., the observed separation between the tips of the patterns agrees reasonably well with the wavelength of the mode of maximum growth,  $\lambda_m$ ), there are a number of unanswered questions [4,5,10]. Most importantly, LSA is limited to early times, so that the questions concerning nonlinear mode interaction cannot be addressed. The computations of the full PDE have been so far limited to narrow domains [11,12]. These computations provide better insight into some of the still open questions (in particular, concerning the influence of wetting properties of a fluid); however small computational domains do not allow for direct comparison with experimental results.

All the theoretical and computational methods require some regularizing mechanism—either assumption of a small foot of fluid in front of the apparent contact line (precursor film), or relaxing the no-slip boundary condition at the fluid-solid interface [13]. Here, we use a precursor film and employ lubrication approximation. Averaging over a short ( $z$ ) direction (perpendicular to the substrate), one obtains a fourth order nonlinear equation of diffusion type for the film height,  $h(x, y)$ ,

$$\frac{\partial h}{\partial t} + \nabla \cdot [h^3 \nabla \nabla^2 h] - D(\alpha) \nabla \cdot [h^3 \nabla h] + \frac{\partial h^3}{\partial x} = 0, \quad (1)$$

where  $\nabla = (\partial_x, \partial_y)$ ,  $D(\alpha) = (3Ca)^{1/3} \cot(\alpha)$ ,  $Ca$  is the capillary number, and  $\alpha$  is the inclination angle. The second term accounts for surface tension, while the two last terms stand for the normal and parallel components of gravity, respectively. Here  $Ca = \mu U / \gamma$ , where  $\mu$  is the fluid viscosity,  $\gamma$  is the fluid-air surface tension, and  $U$  is the velocity scale. The fluid height is scaled by  $h_c$ , the thickness far behind the contact line. Next, we scale the velocity by  $U = \rho g h_c^2 \sin\alpha / 3\mu$ , in-plane coordinates by  $x_c = (h_c a^2 / \sin\alpha)^{1/3}$ , where  $a = \sqrt{\gamma/\rho g}$  is the capillary length, and use the natural time scale  $t_c = x_c/U$  ( $g$  is gravity, and  $\rho$  is the fluid density). We note that the lubrication approximation requires the slope of the free surface to be small; this requirement implies  $[(h_c/a)\sqrt{\sin\alpha}]^{2/3} \ll 1$  (see, e.g., [8]). For small  $\alpha$ 's, this is always fulfilled; however, for large  $\alpha$ 's, it is valid only for very thin films, such as those in [5], where  $h_c/a \approx 0.2$ . We concentrate on this situation and assume that the lubrication approximation is valid; however, we note that this approximation is often used [8–12,14,15] outside its strict range of validity with reasonable success in explaining some of the experimental data.

Our finite difference simulations of the 1D version of (1) led to important conclusions concerning numerical methods [16]. A number of issues related to the accuracy, stability and efficiency have been clarified; in particular, it was shown that a precursor film model performs computationally much better than the slip regularization. For this reason, we use a precursor film model in the 2D simulations where efficiency is crucial.

Our 2D simulations, based on the numerical approach developed in 1D context, are performed in a domain of the size  $[L_x, L_y]$ , with the boundary conditions given by  $h(0, y) = 1$ ,  $h(L_x, y) = b$ ,  $h_x(0, y) = h_x(L_x, y) = 0$ , and  $h_y(x, 0) = h_y(x, L_y) = h_{yyy}(x, 0) = h_{yyy}(x, L_y) = 0$  ( $b$  is the precursor film thickness; we use  $b = 10^{-2}$ ). Most of our simulations are performed on a fixed rectangular grid characterized by  $\Delta x = 0.2$ ,  $\Delta y = 0.25$ . Convergence studies [17] show that this grid size is satisfactory. Time integration uses an implicit second-order accurate scheme; the time step (typically  $\Delta t \approx 10^{-3}$ ) is chosen dynamically based on accuracy requirements. The initial configuration is a well-known traveling wave resulting from 1D simulations (e.g., [8,9]), with the front at  $x_{f0}$ , subject to small perturbations in the  $y$  direction. These perturbations model deviations from the straight front in the experiments. Then, the perturbed front is given by  $x_f(y) = x_{f0} - \sum_{i=1}^N A_i \cos(2\pi y/\lambda_i)$ , where  $A_i$  (we use  $\leq 0.1$ ) is the amplitude of the  $i$ th mode and  $\lambda_i = 2L_y/i$ . In the limit  $N \rightarrow \infty$ , this initial condition is the Fourier expansion of a smoothly corrugated contact line.

We start by simulating a narrow domain of width  $L_y = 16$  (comparable to  $\lambda_m$  from LSA [8,9]), and perturb the contact line by a single mode,  $\lambda = L_y$ . We concentrate on the basic picture of the instability for early and intermediate times, where the results can be compared both with LSA and experiments and do not consider the issues such as recently reported growth saturation for very long times [12].

Figures 1a and 1b follow the evolution of the fluid front as a function of time. For  $D = 0$ , the initial perturbation develops into a long finger, characterized by almost straight sides. In the case  $D = 1$ , however, the normal component of gravity drives lateral spreading, leading to a much wider pattern with oblique sides, consistent with experiments [5,18]. Figure 1c gives the positions of the front,  $x_f$ , and of the trough,  $x_t$ . For early times, we note that the instability develops later for larger  $D$ . For later times, and for  $D = 0$ , the velocities of propagation of fronts,  $v_f$ , and troughs,  $v_t$ , are approximately constant:  $v_f \approx 1.55$ , and  $v_t \approx 0.7$  [the velocity of the unperturbed flow would be  $v = 1 + b(1 + b) \approx 1$ ]. For  $D = 1$ , however,  $v_t$  and  $v_f$  approach each other as time progresses. We note that rather small  $b$ 's ( $b \lesssim 0.02$ ) are needed for the results shown in Fig. 1 to be  $b$  independent; larger  $b$ 's lead to significant changes. In particular, we find that, for larger  $D$ 's, an increase of  $b$  could lead to a transition from unstable to stable regimes, consistently with LSA [10] and weakly nonlinear analysis [14]. The stability boundary in the  $D$ - $b$  space agrees with the result in [3] that predicts that  $D \propto \log(b)$ .

Figure 1d shows the growth rates  $\sigma$ , defined by  $A(t)/A_0 = \exp(\sigma t)$  [ $A(t) = x_f(t) - x_t(t)$ ]. For  $D = 0$  and early times,  $A(t)$  increases exponentially with a

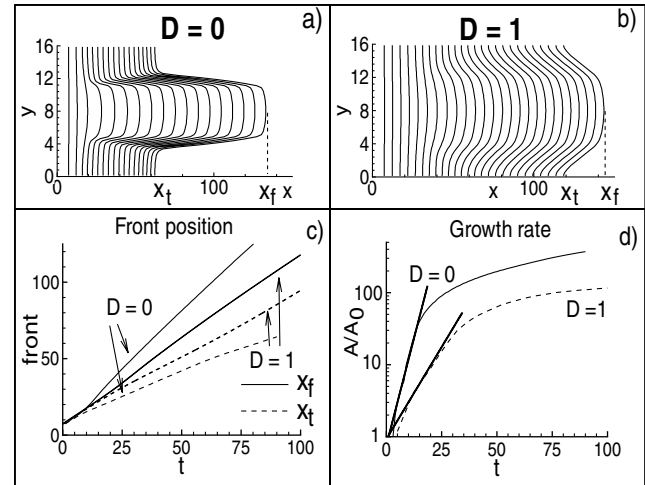


FIG. 1. Snapshots of the contact line shapes (plotted in  $t = 5$  intervals) for the flow down a vertical plane (a), and inclined plane (b). The positions of the fronts and troughs as functions of time (c), and growth rates (d) are also shown; part (d) also shows exponential fits for early times as explained in the text [ $L_x = 40$ ,  $A_0 = A(0) = 0.2$ ].

growth rate close to the one given by LSA [8],  $\sigma \approx 0.24$ . For later times  $A$  increases linearly (at least for the time range considered here), consistent with the qualitative argument given in [15] that predicts a transition from exponential to linear increase of pattern length. For  $D = 1$ , we still obtain exponential growth for early times, now characterized by a smaller growth rate  $\sigma = 0.11$ , as predicted by LSA [10]. For later times, the growth slows down and it becomes even slower than linear. Simulations with intermediate values of  $D$  show that there is a gradual transition between the linear growth for  $D = 0$  and the slower one for  $D = 1$ .

Figure 2 shows the fluid profiles  $h(x, y_0)$  and  $h(x_0, y)$  for  $D = 0, 1$  at a fixed time. The profiles along  $y_0 = 8$  (Figs. 2a and 2c) compare very well with experimental ones in [5]; the profiles along  $y_0 = 0$  show that there is also a (small) bump at the troughs. Figures 2b and 2d show the profiles along the  $y$  direction. In the trough regions ( $x_0 = 48, 146$  for  $D = 0, 1$ , respectively) we see the formation of a valley close to the center, with fluid ridges at the sides. For  $D = 0$ , the profiles midway between the tip and the trough ( $x_0 = 80$ ) can be fitted very well by a constant curvature cylindrical cap, as expected since only capillary forces act in the  $y$  direction. For  $D = 1$  this profile (at  $x_0 = 155$ , Fig. 2d) is flattened due to the normal component of gravity. Very similar profiles are reported in [5], where, for smaller inclination angles, they also observe propagation of the valley to the midway region between tip and trough.

Our boundary conditions at  $x = 0$  specify a “constant flux” situation, where a continuous stream of fluid is assumed. Since most of the experiments were performed with “constant volume,” where a fixed amount of fluid is freed to flow down an incline [1–4,13], we considered that configuration as well. The main differences to the results presented here are associated with the “thinning” of the

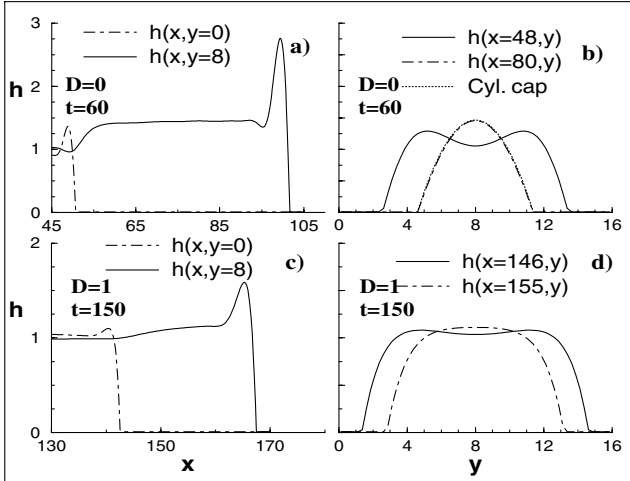


FIG. 2. Thickness profiles of the results from Fig. 1 at a fixed time along  $y = \text{const}$  and  $x = \text{const}$  lines for  $D = 0, 1$ .

fluid far behind the contact line; as shown in [3], both  $D$  and  $b$  become time dependent in this situation, leading to a modified instability mechanism. These questions will be discussed in detail elsewhere [17].

Physical experiments are characterized by wide domains, much larger than  $\lambda_m$ . Also, there is no well-defined perturbation of the contact line at  $t = 0$ ; it is perturbed by noise. We model this noise by perturbing the contact line by a number of modes,  $N$ , characterized by random amplitudes in the range  $[-0.1, 0.1]$ . The results are  $N$  independent as long as  $N$  is sufficiently large.

Figure 3 shows the contour plot of the fluid height for the flow down a vertical plane. In agreement with LSA [8,10] and the experiments [1,5], the short  $\lambda$ 's disappear quickly. For later times, long rivulets form, as reported in [5]. The emerging  $\lambda$ 's (separation between the rivulets) are close to  $\lambda_m$  (LSA). However, LSA applies only to short times and cannot predict the behavior of the system when the perturbations become large. At this point, nonlinear simulations are the only means of linking experiments with theory. Indeed, Fig. 3 recovers results that compare favorably with experimental ones. An example is a natural nonuniformity of the emerging  $\lambda$ 's—the system chooses the most favorable configuration that results from the nonlinear coupling between the initially present modes, modified by the limitations imposed by a finite system size. A similar spread of emerging  $\lambda$ 's is also observed experimentally [1,4,5]. Furthermore, coarsening effects can also be seen in Fig. 3 (e.g., compare the profiles at  $t = 10$  and

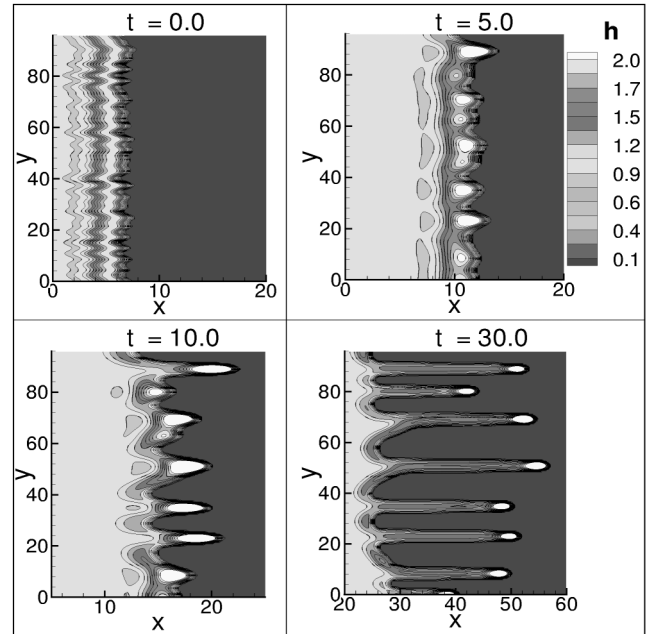


FIG. 3. Contour plot of the fluid height,  $h$ , for the flow down a vertical plane. The contact line is initially perturbed by  $N = 50$  modes, characterized by  $\lambda_i = 2L_y/i$ ,  $i = 1, \dots, 50$ ,  $L_y = 96$ , and  $L_x = 20\text{--}40$  (the domain is increased in the  $x$  direction for long times).

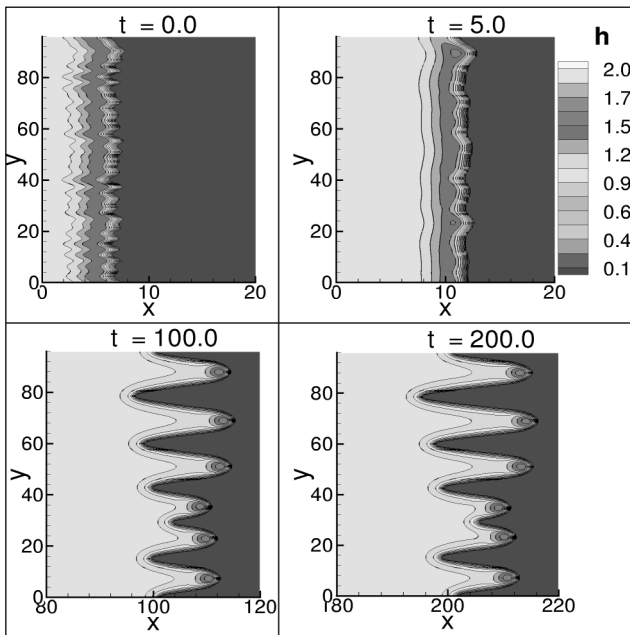


FIG. 4. Contour plot of the fluid height,  $h$ , for the flow down an inclined plane,  $D = 1$ . The initial perturbation is the same as in Fig. 3.

$t = 30$  for  $y \approx 70$ ). If two rivulets initially develop too close to each other, the large curvature in the  $y$  direction forces them to merge.

Figure 4 shows the results for  $D = 1$ . The emerging patterns strongly resemble triangular ones, as observed experimentally [1,4,5]: we also note the formation of valleys across the emerging patterns [5]. The growth of the patterns is slower compared to the  $D = 0$  case, and their separations and widths are increased, even in terms of the length scale  $x_c(\alpha)$ .

From simulations similar to the ones shown in Figs. 3 and 4, we extract results for the average  $\lambda$ 's, and for the width,  $W$ , of the patterns (full width at half length). The detailed analysis and scaling laws for emerging  $\lambda$ 's and  $W$ 's will be given in [17]; here we present the main results. These are computed at late times, where they vary very weakly with time. To ensure that the particular realizations shown in Figs. 3 and 4 were good representatives, we performed additional simulations using different distributions of initial amplitudes, and with different domain sizes ( $L_y = 48, 192$ ). We obtain  $\lambda_{D=0} = 11.8 \pm 2.6$ , and  $\lambda_{D=1} = 16.0 \pm 2.7$  (the average and one standard deviation are reported). These results, obtained for the first time by solving the full PDE (1), agree quantitatively with the experimentally observed ones for “fluid B” in [5,19]. The agreement with experiments strongly supports the basic assumptions of the model, indicating that the nonlinear mode interaction is appropriately described within the lubrication approximation. We note that the average  $\lambda$ 's do not depend on the domain size, and that the relatively large spread of  $\lambda$ 's is not being reduced as the domain size is

increased. These results show that the experimentally observed spread of  $\lambda$ 's is not due to, e.g., boundary effects, but it is an intrinsic property of the system. The widths are given by  $W_{D=0} = 5.5 \pm 0.4$ ,  $W_{D=1} = 11.2 \pm 1.0$ .  $W$ 's are much more uniform than  $\lambda$ 's; this observation is also consistent with experiments [1–5].

In all of our simulations, the troughs move. Consequently, complete coverage of the surface is implied. This suggests that only partially wetting fluids could lead to incomplete coverage. The inclination angle influences the time scale of this coverage and strongly affects the shapes of the emerging patterns: large inclination angles lead to fingerlike rivulets, while smaller ones produce triangular sawtooth patterns. This is supported by recent experiments; however, further experimental and theoretical/computational work is needed to clarify the interplay between wetting properties and gravity. Our computations provide a step in this direction.

The authors would like to thank Andrea Bertozzi for many useful conversations. This work was partially supported by ONR Grant No. N00014-96-1-0656, Consejo Nacional de Investigaciones Científicas y Técnicas (CONICET-Argentina) (J. A. D.), and NJIT Grant No. 421210 (L. K.).

- [1] J. R. de Bruyn, Phys. Rev. A **46**, 4500 (1990); J. M. Jerrett and J. R. de Bruyn, Phys. Fluids A **4**, 234 (1992).
- [2] I. Veretennikov, A. Indekina, and H.-C. Chang, J. Fluid Mech. **373**, 81 (1998).
- [3] Y. Ye and H.-C. Chang, Phys. Fluids **11**, 2494 (1999).
- [4] L. M. Hocking, W. R. Debler, and K. E. Cook, Phys. Fluids **11**, 307 (1999).
- [5] M. F. G. Johnson *et al.*, J. Fluid. Mech. **394**, 339 (1999); M. F. G. Johnson, Ph.D. thesis, Northwestern University, 1997.
- [6] N. Fraysse and G. M. Homsy, Phys. Fluids **6**, 1491 (1994).
- [7] A. M. Cazabat *et al.*, Nature (London) **346**, 824 (1990).
- [8] S. M. Troian *et al.*, Europhys. Lett. **10**, 25 (1989).
- [9] M. A. Spaid and G. M. Homsy, Phys. Fluids **8**, 460 (1996).
- [10] A. L. Bertozzi and M. P. Brenner, Phys. Fluids **9**, 530 (1997).
- [11] L. W. Schwartz, Phys. Fluids A **1**, 443 (1989); D. T. Moyle, M. S. Chen, and G. M. Homsy, Int. J. Multiph. Flow **25**, 1243 (1999).
- [12] M. H. Eres, L. W. Schwartz, and R. V. Roy, Phys. Fluids **12**, 1278 (2000).
- [13] E. B. Dussan V., J. Fluid Mech. **77**, 665 (1976).
- [14] S. Kaliadakis, J. Fluid. Mech. **413**, 355 (2000).
- [15] M. P. Brenner, Phys. Rev. E **47**, 4597 (1993).
- [16] J. Diez, L. Kondic, and A. L. Bertozzi, Phys. Rev. E (to be published).
- [17] L. Kondic and J. Diez (to be published).
- [18]  $D = 1$  corresponds to  $\alpha \approx 20^\circ$  for “fluid B” in [5].
- [19] We performed additional simulations for  $D$ 's in the range  $[0, 2]$  ( $[90^\circ > \alpha > 8^\circ]$  for “fluid B” in [5]); quantitative agreement of computed and experimentally measured  $\lambda$ 's was observed.